$Fe_{1-x}Co_xCl_2$: Competing anisotropies and random molecular fields

P. Wong*
The Department of Physics and The James Franck Institute, The University of Chicago, Chicago, Illinois 60637

P. M. Horn
IBM Thomas J. Watson Research Center, Yorktown Heights, New York 10598

R. J. Birgeneau
Department of Physics, Massachusetts Institute of Technology, Cambridge, Massachusetts 02139

G. Shirane
Brookhaven National Laboratory, Upton, New York 11973
(Received 15 July 1982)

We report a detailed study of the magnetic properties of the site-random solid solution $Fe_{1-x}Co_xCl_2$. $Fe_{1-x}Co_xCl_2$ represents an archetypal example of a system with competing orthogonal spin anisotropies; the easy axis of the Fe spin is orthogonal to the easy plane of the Co spin. The magnetic behavior of single-crystal samples was characterized with the use, as probes, of both dc magnetic susceptibility and elastic neutron diffraction. We find behavior that is in fundamental disagreement with the theoretical predictions for random anisotropy magnets. In particular the transition in one spin component is drastically altered by the existence of long-range order in the other component. We argue that this is due to random off-diagonal terms in the Hamiltonian which generate site-random molecular fields.

I. INTRODUCTION

Following the great success achieved during the past decade in understanding the nature of phase transitions in a wide variety of pure physical systems, it is only natural that more attention is now being focused on the critical and cooperative phenomena in random systems. Magnetic materials with quenched disorder play a special role in these studies since many different types of randomness can be physically realized.[1] Perhaps the most interesting random magnets are compositionally disorderd alloys composed of constituents with dissimilar and/or competing interactions. There are many examples of these: magnetic-nonmagnetic alloys, ferro-antiferromagnetic alloys, alloys with random anisotropies, etc. In almost all cases the competition, in conjunction with the disorder, leads to unusual states of matter. For examples, alloys composed of ferromagnetic and antiferromagnetic constituents can have a spin-glass phase at intermediate concentrations,[1] magnetic-nonmagnetic solid solutions may contain unusual magnetic phases with power-law decay of magnetic correlations,[2] etc. Among all the random magnets, one of the simplest is a solid solution with competing orthogonal site-random anisotropies. In these crystalline binary mixtures there is only compositional disorder which causes the direction of easy axis at each site to depend on the identity of the ion at that site. The work reported in this paper represents a study of the nature of phase transitions and magnetic ordering in an archetypal example of one such system, anhydrous $Fe_{1-x}Co_xCl_2$. A preliminary report of this work has been published elsewhere.[3]

Crystalline $Fe_{1-x}Co_xCl_2$ provides an excellent example of a site-random solid solution with competing spin anisotropies. The easy axis of the Fe spin is orthogonal to the easy plane of Co spin. In Sec. II we give a brief review of the properties of $FeCl_2$ and $CoCl_2$, and explain in more detail why we have chosen this system for study.

According to the theoretical work of Fishman and Aharony (FA),[4] using both a scaling argument and a renormalization-group (RG) calculation, the ordering of the two orthogonal spin components in this type of system should occur independently. The magnetic phase diagram in the x-T plane should consist of two smooth second-order lines crossing each other at a point designated as a "decoupled tetracritical point." This and other more elementary theories will be described in Sec. III. The results of quantitative mean-field calculation pertinent to $Fe_{1-x}Co_xCl_2$ will also be given.

In order to study the properties of $Fe_{1-x}Co_xCl_2$ we have carried out a systematic study of single-crystal samples using as probes both the dc magnetic susceptibility and elastic neutron diffraction over the entire composition range $0<x<1$. The experimental procedures and detailed experimental results are presented in Sec. IV. As will become clear, the simple theories presented in Sec. III fail to describe much of the observed experimental data. In Sec. V we argue for the necessity of including off-diagonal terms in the Hamiltonian and show how these terms lead to the concept of a random molecular field. We will argue that such fields can account for much of the observed experimental data. In Sec. VI we present data on the critical and multicritical behavior of $Fe_{1-x}Co_xCl_2$ with specific emphasis on how these properties might be changed by the off-diagonal terms in the Hamiltonian. Finally, in Sec. VII we discuss the generalization of these results to other systems and present our conclusions.

II. $FeCl_2$ AND $CoCl_2$

A. Crystalline properties

Both $FeCl_2$ and $CoCl_2$ are extensively studied layer-type metamagnets.[5] They have the crystal structure of $CdCl_2$,[6] belonging to the space group $R\bar{3}m$ (D_{3d}^5). The rhombohedral primitive unit cell contains one formula unit, as shown in Fig. 1. The cation is situated at (0,0,0) in the rhombohedral coordinates and the Cl ions at $(u,u,u),(\bar{u},\bar{u},\bar{u})$ where $u\simeq 0.25$. A simpler way to view this structure is to observe that every cation layer is sandwiched between two Cl layers. The sandwiches are stacked in a 12312... sequence as indicated in Fig. 1, that is, one has an fcc stacking sequence with alternate cation sheets removed along the trigonal [111] axis. The two-dimensional lattice within each layer is triangular. It is therefore more convenient to use hexagonal coordinates with lattice vectors related to the rhombohedral ones by $\vec{x}_h=\vec{x}_r-\vec{y}_r$, $\vec{y}_h=\vec{y}_r-\vec{z}_r$, $\vec{z}_h=\vec{x}_r+\vec{y}_r+\vec{z}_r$. The hexagonal primitive unit cell then contains three formula units with the cations at (0,0,0), $(\frac{1}{3},\frac{2}{3},\frac{2}{3})$, and $(\frac{2}{3},\frac{1}{3},\frac{1}{3})$. It is not difficult to see from Fig. 1 that the separation between two Cl layers is twice that between a cation layer and a Cl layer. This causes the binding between adjacent Cl layers to be very weak so that the crystal is lamellar in habit and quite soft.

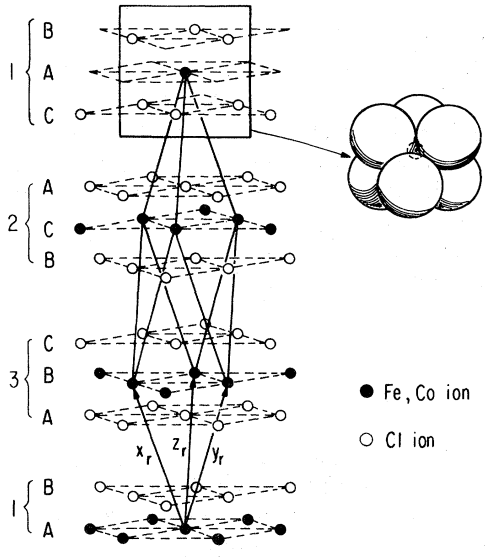

FIG. 1. Crystal structure of $FeCl_2$ and $CoCl_2$. The crystal field on the magnetic ion is primarily due to six Cl ions around it in an approximate octahedral arrangement.

The important physical parameters of $FeCl_2$ and $CoCl_2$ are summarized in Table I. Their lattice constants match within 1%, ensuring that the *random* solid solution $Fe_{1-x}Co_xCl_2$ can be formed at any composition x without altering the crystal structure. Their melting points are 675 and 725 °C, respectively, indicating little difference in their cohesive energy. When a crystal is grown from the melt[7] near 700°C, this small difference ($\sim$50 °C) cannot lead to any appreciable local segregation. However, during crystal growth a macroscopic composition gradient develops along the crystal's growth direction. Detailed chemical analysis of our samples shows that this gradient in x can be as large as 0.01/cm, a fact of important positive consequences for our neutron-diffraction studies.

B. Magnetic properties

Early neutron-diffraction work by Wilkinson *et al.*[8] had shown that both $FeCl_2$ and $CoCl_2$ ordered ferromagnetically within the layer and antiferromagnetically between adjacent layers. The difference between the two magnetic structures is that the Fe spins order along the hexagonal c axis while the Co spins order in the a-b plane perpendicular to it. The in-plane anisotropy for the Co spins is relatively small. It is known that an applied field of 2 kOe in the a-b plane induced a spin-flop (SF) transition[8] and 33 kOe is sufficient to saturate the magnetization.[9] The maximum in-plane anisotropy field (H_A) can be deduced from the relation $H_{SF}=(2H_AH_E)^{1/2}$, giving $H_A\lesssim 100$ Oe. The actual anisotropy field is probably much smaller since the spin-flop transition is at least partially resisted by domain effects, not just by spin anisotropy. Therefore, the Co spins are essentially XY-like and the Fe spins are Ising-type. These anisotropies are due to the crystal-field sym-

TABLE I. Important physical parameters for $FeCl_2$ and $CoCl_2$.

		$FeCl_2$	$CoCl_2$
Hexagonal lattice constants	a_h	3.579 A	3.544 A
($T=300$ K)	c_h	17.536 A	17.430 A
Rhombohedral lattice parameters	a_r	6.20 A	6.16 A
($T=300$ K)	α_r	33°33′	32°26′
Molecular weight		126.76	129.84
Density (g/cm^3)	ρ	3.25	3.41
Melting point (°C)		675	725
Color		brown	blue
Magnetic moment	μ	$\sim 4\mu_B$	$\sim 3\mu_B$
Effective spin	S	1	$\frac{1}{2}$
Néel temperature (K)	T_N	23.6	24.7
Exchange constants (K)[a]	$J_{\|\|}$	5.53	5.68
	$J_\perp$	3.60	15.33
	J	4.24	12.11
	D	1.29	−6.44

[a]The exchange constants are defined according to Eqs. (1) and (2).

metry of surrounding ions as well as to spin-orbit interaction within the cations themselves. Both factors are basically unchanged in the mixed crystals and the single-ion anisotropies should remain the same.

It can be seen in Fig. 1 that every cation is surrounded by six Cl ions in an octahedral arrangement with a trigonal distortion. According to Hund's rule, the ground term for Fe^{2+} $3d^6$ ion is ^5P and for Co^{2+} $3d^7$ is ^4F. A number of crystal-field-theory calculations on these ground terms exist.[10–14] The general conclusion is that the Fe ion has a triplet ground state and Co ion has a doublet ground state, appropriate to the pseudospin assignment $S^F=1$, $S^C=\frac{1}{2}$.

The magnetic exchange interaction within these ground states can then be described by the diagonal pseudospin Hamiltonian

$$\mathcal{H}=-2\sum_{\langle ij\rangle} J_{||}^{ij}\vec{S}_{||}(i)\cdot\vec{S}_{||}(j)+J_{\perp}^{ij}\vec{S}_{\perp}(i)\cdot\vec{S}_{||}(j)\ , \quad (1)$$

or equivalently

$$\mathcal{H}=-2\sum_{\langle ij\rangle} J^{ij}\vec{S}(i)\cdot\vec{S}(j) + D^{ij}[\vec{S}_{||}(i)\cdot\vec{S}_{||}(j)-\tfrac{1}{2}\vec{S}_{\perp}(i)\cdot\vec{S}_{\perp}(j)]\ , \quad (2)$$

where the || and ⊥ signs are with respect to the hexagonal c axis. The anisotropy is represented by the fact that the $J_{||}^{FF}>J_{\perp}^{FF}$ ($D^{FF}>0$) between the two Fe spins, and $J_{||}^{CC}<J_{\perp}^{CC}$ ($D^{CC}<0$) between the Co spins. The exchange constants for the first, second, and third neighbors (J_1,J_2,J_3) have been determined from the spin-wave dispersion relations[10,14] and antiferromagnetic resonance measurements.[9] The important physical parameters of pure $FeCl_2$ and $CoCl_2$ are listed in Table I. We note that the strength of interaction between Co spins is comparable to that between Fe spins. Concomitantly, their Néel temperatures are approximately the same. In addition, the anisotropies (D) in both systems are very strong, comparable to the exchange (J). Both features are important in studying the effect of competing random anisotropies. We should note that while the above Hamiltonian has heretofore been sufficient to describe the salient behavior of the pure systems, in Sec. V we will argue for the necessity of including off-diagonal terms to describe our results on the $Fe_{1-x}Co_xCl_2$ system.

Finally, we point out that the interlayer exchange is only an order of magnitude smaller than the intralayer exchange,[5,10] not sufficiently weak for any quasi-two-dimensional critical behavior. Yelon and Birgeneau[15] have studied the spin-spin correlation above the Néel transition in $FeCl_2$. They find that the correlation lengths parallel and perpendicular to the c axis are of comparable magnitude and the critical behavior is fully three dimensional. Although similar studies on $CoCl_2$ or $Fe_{1-x}Co_xCl_2$ have not been made, there is no reason to suspect otherwise.

III. THEORY

In order to facilitate the interpretation and discussion of our experimental results, we describe in this section three existing theories that are relevant to the random anisotropy problem. Although these theories differ in both approach and complexity, there are some important common features among them.

A. Landau theory

The simplest theory for systems with two competing order parameters is a purely phenomenological one due to Liu and Fisher.[16] If the order parameters are the two orthogonal components of magnetization $M_{||}$ and $M_{\perp}$, the free energy can be written as a standard Landau expansion:

$$F(x,H,T)=aM_{||}^2+bM_{\perp}^2+cM_{||}^4+2dM_{||}^2M_{\perp}^2 +eM_{\perp}^4+\cdots , \quad (3)$$

where all the coefficients a,b,c,d,e presumably depend on the alloy compositions x. As in the case of one order-parameter Landau theory, one assumes

$$a=a_0(T-T_{||}) ,$$

$$b=b_0(T-T_{\perp}) ,$$

where $a_0>0$, $b_0>0$. $T_{||}$ and $T_{\perp}$ also depend on x and represent the transition temperatures of $M_{||}$ and $M_{\perp}$ when there is no coupling between them ($d=0$). Following the usual procedure of minimizing the free energy in Eq. (3), it can be shown that there are four sets of possible solutions representing the different phases of the system. They are the following: (a) paramagnetic phase: $M_{||}=0$, $M_{\perp}=0$; (b) $||$-ordered phase: $M_{||}=\sqrt{-a/2c}$, $M_{\perp}=0$; (c) $\perp$-ordered phase: $M_{||}=0$, $M_{\perp}=\sqrt{-b/2e}$; (d) mixed phase: $M_{||}^2=(bd-ae)/2(ce-d^2)$, $M_{\perp}^2=(ad-bc)/2(ce-d^2)$.

Depending on x and T, one of these phases will have the lowest free energy. The possible phase diagrams resulting from this calculation are depicted in Figs. 2(a)–2(d). They depend critically on the coupling constant d.

(a) $d=0$ [Fig. 2(a)]: With no interaction between the two order parameters, the phase boundaries are just two smooth lines defined by $a=0$, $b=0$.

(b) $d<0$ and $d^2<ce$ [Fig. 2(b)]: Simultaneous ordering of $M_{||}$ and $M_{\perp}$ is favored and the mixed-phase region is expanded as compared to Fig. 2(a).

(c) $d>0$, $d^2<ce$ [Fig. 2(c)]: The two order parameters are repulsive to each other; the mixed-phase region is reduced compared to Fig. 2(a).

(d) $d>0$ and $d^2>ce$ [Fig. 2(d)]: $M_{||}$ and $M_{\perp}$ are strongly repulsive. They cannot order simultaneously and the mixed phase is unstable. The $||$- and $\perp$-ordered phases are separated by a first-order line EM defined by $a^2/c=b^2/e$. As with all first-order transitions, there is a metastable region near this line bounded by the two dashed lines in Fig. 2(d). As we shall see in the following, phase diagrams predicted by other theories generally fall into one of the above categories.

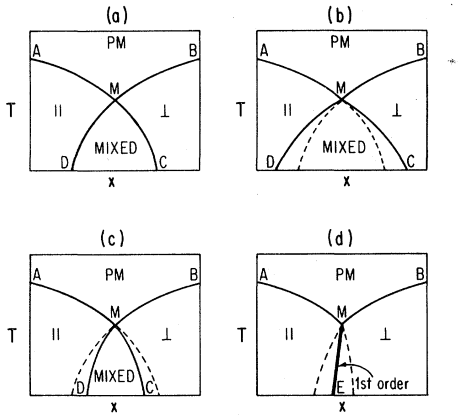

FIG. 2. Four possible magnetic phase diagrams in the Landau theory of Liu and Fisher: (a) zero coupling ($d=0$); (b) attractive order parameters ($d>0$ and $d^2<ce$), dashed line corresponds to zero coupling ($d=0$); (c) repulsive order parameters ($d>0$ and $d^2<ce$), dashed line corresponds to zero coupling ($d=0$); (d) strongly repulsive order parameters ($d>0$ and $d^2>ce$), dashed line corresponds to weakly repulsive order parameters.

B. Mean-field theory (MFT)

A more quantitative theory is due to Matsubara and Inawashiro[17] (MI) who considered the solid solution of a spin-1 ion and a spin-$\frac{1}{2}$ ion with orthogonal anisotropies, exactly the situation of $Fe_{1-x}Co_xCl_2$. They neglected the random local environment of the individual ion and assumed that the molecular fields acting on similar ions are identical; the field is simply weighted by the solution's average compositions. For example, the α component of the molecular field on an Fe ion is

$$h_{\alpha}^F=2z[(1-x)J_{\alpha}^{FF}\langle S_{\alpha}^F\rangle+xJ_{\alpha}^{FC}\langle S_{\alpha}^C\rangle] , \quad (4)$$

and similarly for the Co ion. Their calculation demonstrated a phase diagram similar to Fig. 2(c). Substituting the values of $J_{\perp}$ and $J_{||}$ in Table I and assuming

$$J^{FC}=(J^{FF}J^{CC})^{1/2} \quad (5)$$

in MI's result, one can obtain

$$T_{||}=44.2-27.2x , \quad (6a)$$

$$T_{\perp}=46.0-17.2(1-x) \quad (6b)$$

as the upper phase boundaries. The linearity here is a direct consequence of the assumption in Eq. (5), which is approximately true at best. Since the mean-field transition temperatures 44.2 and 46.0 K for $x=0$ and in Eq. (6) are well above the experimental values of 23.6 and 24.7 K for pure $FeCl_2$ and $CoCl_2$, we normalize Eq. (6a) at $x=0$, and Eq. (6b)

at $x=1$. This gives

$$T_{||}=23.6-14.5x\ , \tag{7a}$$

$$T_{\perp}=24.7-9.24(1-x)\ . \tag{7b}$$

The multicritical point is the intersection of these two lines, which occurs at

$$x_M=0.343\ ,\qquad T_M=18.6\ , \tag{8}$$

where T_M is measured in K.

At $T=0$ the mixed phase occurs between $x=0.287$ and 0.452 as shown by points D' and C', the solid lines in Fig. 3. That this phase diagram is similar to Fig. 2(c) and corresponds to the case of weak repulsive coupling between the two order parameters is quite reasonable, because in Eq. (4) the components of $\langle\vec{S}^F\rangle$ and $\langle\vec{S}^C\rangle$ are always coupled. Furthermore, it can be shown from MI's result that the mixed phase is always physically stable over some range of x at zero temperature.

C. Modern theory

As shown in Fig. 3, the phase boundaries calculated by MFT consist of four critical lines meeting at a point, known as a tetracritical point. MFT predicts that the phase boundaries intersect at the tetracritical point at finite angles. In pure systems taking fluctuations into account generally modifies the phase boundaries to meet tangentially at a multicritical point.[18–21] However, for the random system considered here, Fishman and Aharony[4] (FA) argue that the coupling between the two order parameters is irrelevant. Therefore, near the multicritical point (MCP) the phase diagram should have the topology of Fig. 2(a) and consist of only two smooth lines crossing at a so-called "decoupled tetracritical point."

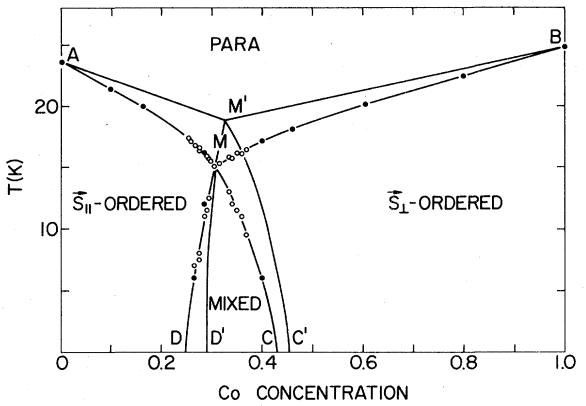

FIG. 3. Magnetic phase diagram of $Fe_{1-x}Co_xCl_2$. The solid lines *AM'C'* and *BM'D'* are calculated by mean-field theory; solid lines *AMC* and *BMD* are guides to the eye constructed from experimental points; solid circles obtained from susceptibility data, open circles from neutron scattering (see text).

Briefly, FA arguments are based on the observation that the coupling between $\vec{S}_{||}$ and $\vec{S}_{\perp}$ has the form of an energy-energy coupling. Near the phase transition, it has a temperature dependence of $t^{1-\alpha_{||}}t^{1-\alpha_{\perp}}$, where t is the reduced temperature and the α's are the specific heat exponents for $\vec{S}_{||}$ and $\vec{S}_{\perp}$. If ξ is the correlation length ($\xi\sim t^{-\nu}$), then in d dimensions the coupling term for a correlated cluster of size ξ^d is proportional to $t^{-d\nu}t^{1-\alpha_{\perp}}t^{1-\alpha_{||}}$. With the use of the hyperscaling relationship $d\nu=2-\alpha$ one obtains a coupling term $\sim t^{-(1/2)(\alpha_{||}+\alpha_{\perp})}$. Clearly, if both $\alpha_{||}$ and $\alpha_{\perp}$ are negative, the coupling approaches zero as $t\to 0$. Since it is commonly believed that $\alpha<0$ is always true in random systems,[22] FA conclude that the coupling is irrelevant, and the two order parameters are uncoupled near the tetracritical point. However, several difficulties should be noted. First, while the phase boundaries are predicted to cross smoothly as in Fig. 2(a), the coupling goes to zero only as $t\to 0$, and hence far below the multicritical point the repulsive nature of the two order parameters will lead to a reduced mixed-phase region as in Fig. 2(c). Second, although the specific-heat exponent for the random Ising model ($\alpha_{||}$) is negative, in the pure system $\alpha_p=+\frac{1}{8}$. According to the argument by Harris,[22] the crossover from pure to random behavior occurs only in the reduced temperature range $t\lesssim[c(1-c)]^{1/\alpha_p}$, where c is the concentration of broken bonds. In the best situation ($c=0.5$) this still requires $t\lesssim 10^{-5}$. Therefore, it is doubtful that the decoupled behavior can ever be observed experimentally. Finally, we emphasize that FA's theory is based on the simple diagonal exchange Hamiltonian in Eq. (1) and we shall argue in Sec. V that additional off-diagonal terms must be included for symmetry reasons.

IV. EXPERIMENT

A. Magnetic susceptibility

To study the systematic variation of anisotropy with composition, magnetic susceptibilities parallel and perpendicular to the c axis ($\chi_{||}$ and $\chi_{\perp}$) were measured by the conventional Faraday's method. Eight samples were measured altogether, covering the composition range $0.1\lesssim x\lesssim 0.8$.

The large susceptibility of $Fe_{1-x}Co_xCl_2$ makes possible the use of relatively small samples which in turn reduces the problem of composition gradients. The samples were small platelets typically 20 mg in

weight and $2.5\times2.5\times1.0$ mm^3 ($w\times l\times t$) in dimension. The detail of sample preparation is described elsewhere.[7] The average value of x of each sample was analyzed by atomic absorption spectrophotometry accurate to 0.001. Monotonic variation of x across the sample was estimated to be 0.005 maximum. Since these materials are quite hygroscopic, most of the handling was done inside a glove bag. After weighing, the crystals were coated with a thin layer of Apiezon AP 100 grease to protect them from moisture.

A single-crystal sample, with its c axis oriented vertically, was suspended in an inhomogeneous magnetic field. The vertical force on the sample was measured by a Cahn RG microbalance. The gradients $dH_{||}^2/dz$ and $dH_{\perp}^2/dz$ were determined by a reference sample of known susceptibility. $\chi_{||}$ and $\chi_{\perp}$ could be measured in absolute magnitude by applying the field either vertically or horizontally. In both cases the gradient dH^2/dz was of order 10^4 Oe^2/cm and H was not more than a few hundred gauss, well within the sample's linear response region. The sample was placed in a copper holder and suspended by a fine tungsten wire (0.8 mil). The typical measured force was in the range of 0.1—1.0 mg, giving the susceptibility less than 1% error. Two indepdently powered nichrome heaters and a copper-Constantan differential thermocouple helped to control the temperature and its gradient. Near the sample a vertical gradient of less than 0.1 K/cm was maintained throughout the experiment. The absolute temperature uncertainty at the sample position is estimated to be ~0.1 K.

There are several difficulties and limitations in our measurement that should be mentioned. First, the sample was oriented only to within an estimate error of a few degrees. One can easily show that for an angular error θ the subsequent error in $\chi_{||}$ or $\chi_{\perp}$ is only $|\chi_{||}-\chi_{\perp}|\sin^2\theta$. For $\theta\lesssim5°$, this is not significant. Second, the applied field always has a slight horizontal gradient in addition to the vertical one and tends to move the sample sideways. We reduced this movement by using a copper sample holder approximately 30 times the weight of the sample. The maximum horizontal displacement was about 1 mm and judged unimportant. Finally, one must also take into account demagnetization effects. Since χ is quite large for $Fe_{1-x}Co_xCl_2$, especially near the Neél transition, such effects can be of the order of 10%. Unfortunately, since the samples do not have a simple geometry and further can rotate horizontally in the magnetic field, it is difficult to correct quantitatively for this effect. We stress, however, that the conclusions we shall draw from the data are based on the qualitative shape of $\chi(T)$ and hence not sensitive to these details.

Molar susceptibilites between 4.5 and 80 K were obtained in this experiment. We find the high-temperature data ($\chi<0.3$ emu/mole) to be quite accurately fitted by the Curie-Weiss form

$$\chi=\frac{C}{T-T_c}\ . \tag{9}$$

The fitting parameters are summarized in Table II, along with the samples' compositions and their transition temperatures.

Typical results between 4.5 and 50 K are shown in Figs. 4(a)—4(h). We note that the data for the $x=0.0977$ sample in Fig. 4(a) is similar to that of the pure $FeCl_2$ measured by Brandt[23] and Trapp[24]; $d\chi_{||}/dT$ is sharply peaked indicating spin ordering in the c direction. On the other hand, the data of the $x=0.8011$ sample in Fig. 4(h) is similar to that of the pure $CoCl_2$ measured by Hsu[13]; $d\chi_{\perp}/dT$ is sharply peaked, indicating spin ordering in the a-b plane. At intermediate compositions there is a clear systematic variation. Figs. 4(c)—4(f) show peaks in both $\chi_{||}$ and $\chi_{\perp}$. The ones at high temperature (T_H) are quite sharp indicating well-defined phase transitions and good sample homogeneity. In contrast, the ones at lower temperature (T_L) are always very broad, not at all typical of a second-order transition. For pedagogical purposes it is useful to remember that near phase transitions the magnetic susceptibility of an antiferromagnetic is a measure of the ordering energy. Hence the temperature derivative of the susceptibility is proportional to the magnetic specific heat.[26] The behavior observed in the samples of intermediate concentration suggests that when one spin component (either $\vec{S}_{||}$ or $\vec{S}_{\perp}$) is ordered, it forces the other component to form antiferromagnet spin clusters (or domains). The loss of entropy as these clusters grow is a gradual one and is reminiscent of the Schottky-type behavior of the specific heat of a spin-glass. More will be said about this later.

If we define the transition temperature by the maximum in $d\chi/dT$ regardless of how rounded it is, a phase diagram can be constructed, as depicted in Fig. 3. The phase diagram clearly resembles the tetracritical phase diagrams discussed in Sec. III. In what follows we will define the temperature of the upper transition lines AM and MB as $T_H(x)$ and the lower lines MD and MC as $T_L(x)$. We reiterate, however, that the low-temperature lines are not well defined and correspond only to a gradual ordering process.

B. Neutron scattering

Neutron-diffraction experiments were carried out at the High Flux Beam Reactor of the Brookhaven

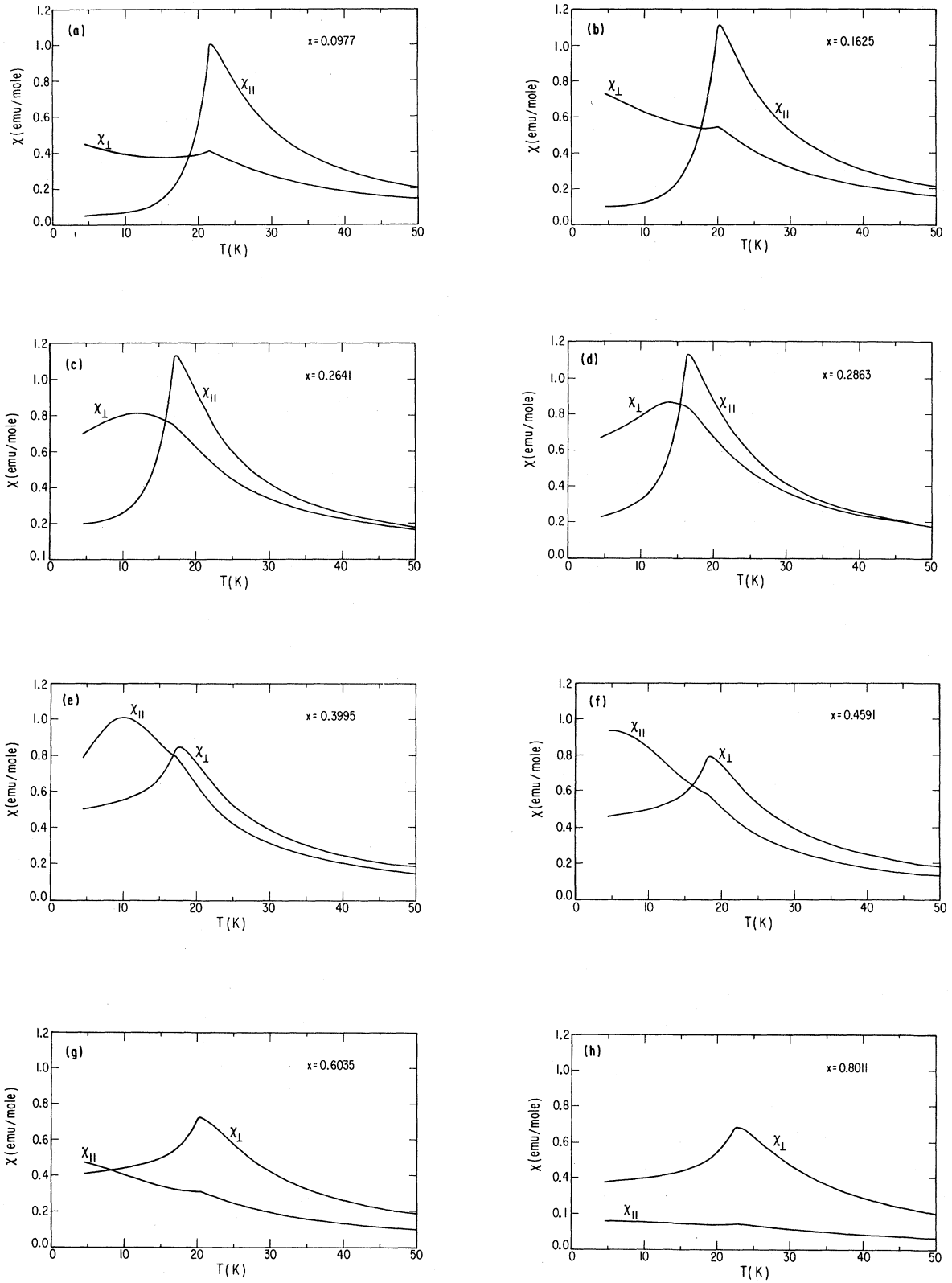

FIG. 4. Temperature dependence of the molar magnetic susceptibilities parallel ($\chi_{||}$) and perpendicular ($\chi_{\perp}$) to the c axis in eight samples of different compositions.

TABLE II. Summary of susceptibility results.[a]

Sample	Co concentration x (±0.001)	Transition temperature upper T_H (K) (±0.1 k)	Transition temperature lower T_L (K) (±1.0 K)	Curie temperature $T_c^{\parallel}$ (K)	Curie temperature $T_c^{\perp}$ (K)	Curie constant $C^{\parallel}$	Curie constant $C^{\perp}$	Effective Bohr magneton $p^{\parallel}$	Effective Bohr magneton $p^{\perp}$
$FeCl_2$[b]	0	23.6		~26.0	~8.0	~5.0	~4.5	~6.32	~6.00
1	0.0977	21.4		21.85(34)	9.51(19)	5.91(6)	5.72(3)	6.87	6.76
2	0.1625	20.0		19.75(34)	9.66(20)	6.40(6)	6.49(3)	7.16	7.20
3	0.2641	16.8	6.0	18.33(35)	11.40(19)	5.72(6)	6.35(3)	6.76	7.13
4	0.2863	16.2	12.0	19.30(47)	11.68(21)	5.55(7)	6.81(4)	6.66	7.38
5	0.3995	17.2	6.0	15.51(32)	13.69(16)	5.09(4)	6.61(3)	6.38	7.27
6	0.4591	18.1		13.31(20)	14.84(19)	4.75(2)	6.25(4)	6.16	7.07
7	0.6035	20.1		9.64(24)	15.41(11)	4.07(2)	6.46(2)	5.70	7.19
8	0.8011	22.4		1.02(14)	17.20(10)	3.25(1)	6.62(2)	5.10	7.27
$CoCl_2$[c]	1.000	24.7			~18.5		~4.9		~6.26

[a]The composition x is determined by atomic absorption analysis. T_H and T_L are determined from the maxima of $d\chi_{\parallel}/dT$ and $d\chi_{\perp}/dT$ in the data. The last six columns are the results of least-squares fits to the high-temperature data.
[b]Value of T_H is taken from Ref. 15. $T_C^{\parallel}$, $C^{\parallel}$, and $p^{\parallel}$ are derived from the data listed in Ref. 23. $T_C^{\perp}$, $C^{\perp}$, and $p^{\perp}$ are derived from the data of Ref. 24.
[c]Value of T_H is taken from Ref. 25. $T_C^{\perp}$ and $p_{\perp}$ are derived from the data of Ref. 13.

National Laboratory using 13.6-meV neutrons. All measurements were made on a triple-axis spectrometer, set for elastic scattering. Angular collimation of the beam varied depending on the comparative needs of intensity and resolution.

The samples were mounted with their a^*-c^* axes in the horizontal scattering plane; this oriented the cylindrical growth axis approximately vertical. The samples were then masked in such a way that the neutrons illuminated only a small vertical fraction of the sample; within the illuminated volume the variation in concentration x was typically 0.5 at.%. The concentration to be studied could then be varied continuously by moving the position of the mask vertically. The range of x for each sample was determined by atomic absorption spectrophotometry and the average concentration $\bar{x}$ for each measurement was estimated according to the mask position. However, since the positional relationship between the mask and sample could not be established exactly, the absolute value of $\bar{x}$ can have an error as much as 0.01. The mosaic distribution of the a-b planes is typically 1° full width at half maximum, asymmetric, and multiply peaked. Most samples consist of two crystalline domains with a common c axis but rotated by 60° about it. The scattering geometry together with the magnetic and nuclear reciprocal lattice points (rlp) in the a^*-c^* plane are shown in Fig. 5.

The magnetic neutron scattering cross section for energy-momentum transfer ω and q is given by[27]

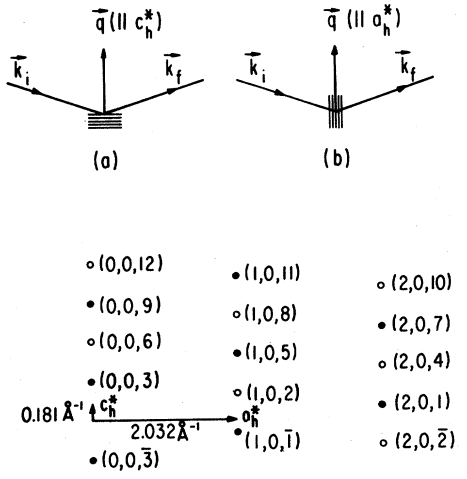

FIG. 5. Magnetic (●) and nuclear (○) reciprocal-lattice points of $FeCl_2$ and $CoCl_2$ in the a^*-c^* plane.

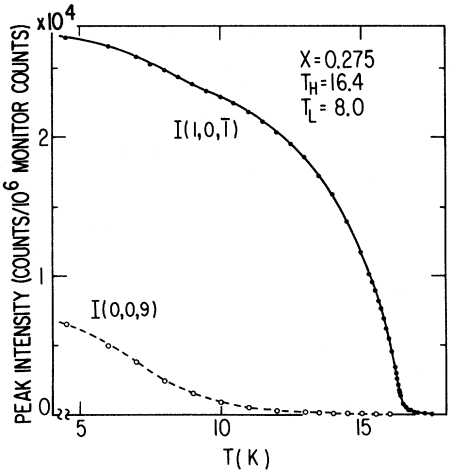

FIG. 6. Peak intensity vs temperature for concentration $x=0.275$.

TABLE III. Summary of neutron scattering results from sixteen measurements of six different samples. The compositions are estimated from atomic absorption analyses made on different parts of each sample. T_H and T_L are determined by the peak and wing intensity data. β, D, and T_c are the result of least-squares fits to the peak intensity data. The last two columns are the conditions of the fit.

Sample number	x	T_H	T_L	β	D	T_c	Temperature range (t)	χ^2
9	0.275	16.40 ±0.05	8.0 ±0.5	0.290 ±0.010	1.41 ±0.10	16.36 ±0.02	0.004–0.15	1.2
10	0.266	16.80 ±0.10	7.0 ±0.5					
11	0.255	17.35 ±0.10		0.265 ±0.01	1.34 ±0.10	17.28 ±0.05	0.009–0.13	1.4
12	0.400	17.20 ±0.05		0.310 ±0.01	1.27 ±0.10	17.19 ±0.02	0.004–0.016	1.5
13	0.295	15.60 ±0.05	12.5 ±0.5					
14	0.340	15.70 ±0.10	12.0 ±1.0					
15	0.360	16.10 ±0.05	11.0 ±0.5					
16	0.369	16.35 ±0.10	9.5 ±0.5					
17	0.350	16.15 ±0.15	11.5 ±0.5	0.327 ±0.02	1.3 ±0.1	16.16 ±0.05	0.004–0.14	1.4
18	0.335	15.75 ±0.05	13.0±0.5	0.322 ±0.015	1.3 ±0.1	15.72 ±0.05	0.003–0.11	.7
19	0.315	15.30 ±0.10						
20	0.291	15.95 ±0.05	11.5 ±0.5					
21	0.293	±0.10	15.70					
22	0.258	17.10 ±0.10	<5.0					
23	0.275	16.50 ±0.10	7.5±1.0					
24	0.286	15.90 ±0.10	11.0 ±0.5					

$$\frac{d^2\sigma}{d\omega\, dq} = \left[\frac{g_N e^2}{2m_e C^2}\right]^2 [\tfrac{1}{2}F(\vec{q})]^2 \times \sum_{\alpha,\beta=1}^{3} (\delta_{\alpha\beta} - \vec{q}_\alpha \vec{q}_\beta)\mathcal{S}_{\alpha\beta}(\vec{q},\omega), \quad (10)$$

where $\mathcal{S}_{\alpha\beta}(\vec{q},\omega)$ is the Fourier transform of the space-time spin-spin correlation function

$$\mathcal{S}_{\alpha\beta}(\vec{r},t) \equiv \langle M_\alpha(0,0) M_\beta(\vec{r},t)\rangle .$$

For elastic scattering, $\omega = 0$. The coherent part (Bragg scattering) is proportional to the square of the order parameters $M_{||}$ [$\equiv g_{||}\langle \vec{S}_{||}(\vec{q}_B)\rangle$] and $M_\perp$ [$\equiv g_\perp \langle \vec{S}_\perp(\vec{q}_B)\rangle$], where $\vec{q}_B$ is the Bragg wave vector. The incoherent part (diffuse scattering) is related to the wave-vector–dependent susceptibilities $\chi_{\alpha\beta}(\vec{q})$, etc. Most of our data were taken at rlp (0,0,9), (0,0,3), and (1,0,$\bar{1}$).[17] With the use of Eq. (10), the intensity gives

$$I(0,0,9) \propto I(0,0,3) \propto \mathcal{S}_{xx}(\vec{q}) + \mathcal{S}_{yy}(\vec{q}) , \quad (11a)$$

$$I(1,0,\bar{1}) \propto 0.992\mathcal{S}_{zz}(\vec{q}) + \mathcal{S}_{yy}(\vec{q}) + 0.008\mathcal{S}_{xx}(\vec{q}) . \quad (11b)$$

Thus the Bragg intentisy (I_B) gives

$$I_B(0,0,9) \propto I_B(0,0,3) \propto M_\perp^2 , \quad (12a)$$

$$I_B(1,0,\bar{1}) \propto 0.992M_{||}^2 + 0.504M_\perp^2 \simeq M_{||}^2 + \tfrac{1}{2}M_\perp^2 . \quad (12b)$$

In most cases, only the peak intensity of each reflec-

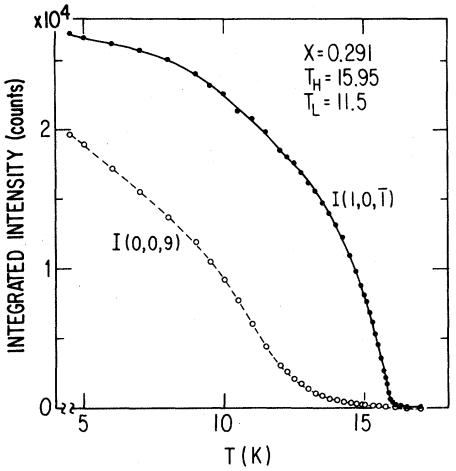

FIG. 7. Integrated intensity vs temperature for concentration $x=0.291$.

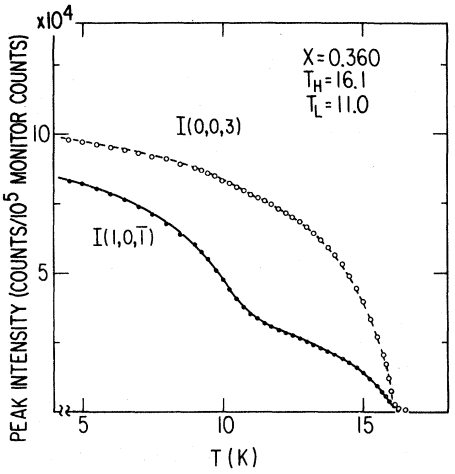

FIG. 9. Peak intensity vs temperature for concentration $x=0.360$.

tion was measured, but in some very thin samples ($\lesssim 1$ mm thick), in which we noticed a slight shifting of mosaicity with temperature, the intensity was integrated over ϕ scans.

The diffuse scattering intensity (I_D) is much weaker than I_B below the transition. It must be measured at a wing position far enough away from the Bragg peak to give the behavior of $\chi(\vec{q})$, e.g.,

$$I_D(0,0,9,+\delta) \propto \chi_{xx}(\vec{q})+\chi_{yy}(\vec{q})=2\chi_{\perp}(\vec{q}) , \tag{13a}$$

$$\begin{aligned} I_D(1+\eta,0,\bar{1}) &\propto 0.992\chi_{zz}(\vec{q})+\chi_{yy}(\vec{q}) \\ &\quad +0.008\chi_{xx}(\vec{q}) \\ &\simeq \chi_{||}(\vec{q})+\chi_{\perp}(\vec{q}) . \end{aligned} \tag{13b}$$

Here $\vec{q}$ is a wave vector slightly away from $\vec{q}_B$; i.e., $\vec{q}=\vec{q}_B+\delta\vec{q}$. Thus for measuring $\chi_{\perp}$ in Eq. (13a), $\delta\vec{q}$ was in the direction of c^*, while for measuring $\chi_{\perp}+\chi_{||}$ in Eq. (13b), $\delta\vec{q}$ was in the direction of a^*. This was to avoid the Bragg contribution due to the poor sample mosaicity.

A total of nine samples were surveyed. Data were taken from several different segments of each sample. In Table III we list sixteen cases from six samples which were studied in detail. In Figs. 6–10 we show the temperature dependence of the scattered intensity at the (1,0,$\bar{1}$) and (0,0,9) [or equivalently (0,0,3)] magnetic reflections for five different samples. In Figs. 6 and 7, where $x=0.275$ and 0.291,

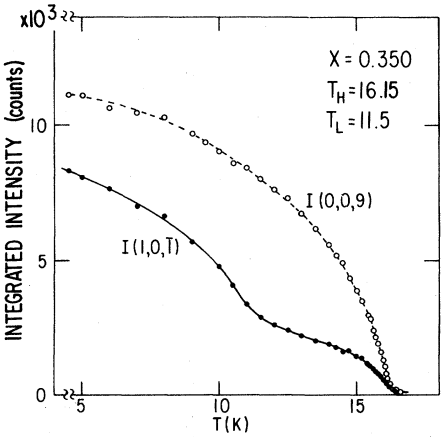

FIG. 8. Integrated intensity vs temperature for concentration $x=0.350$.

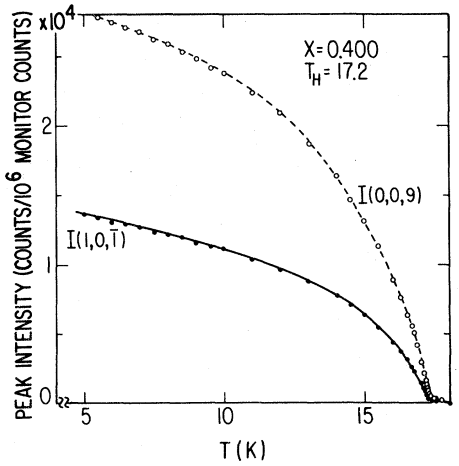

FIG. 10. Peak intensity vs temperature for concentration $x=0.400$.

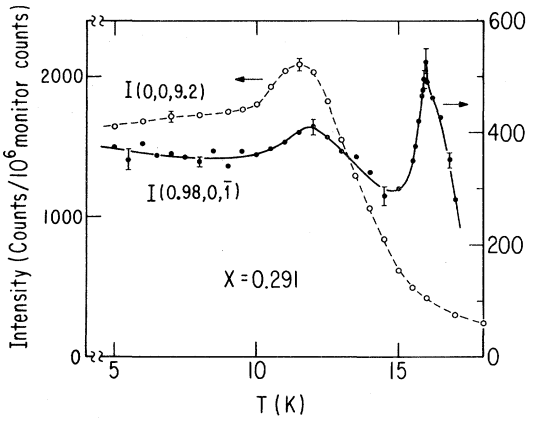

FIG. 11. Wing intensity vs temperature for concentration $x=0.291$.

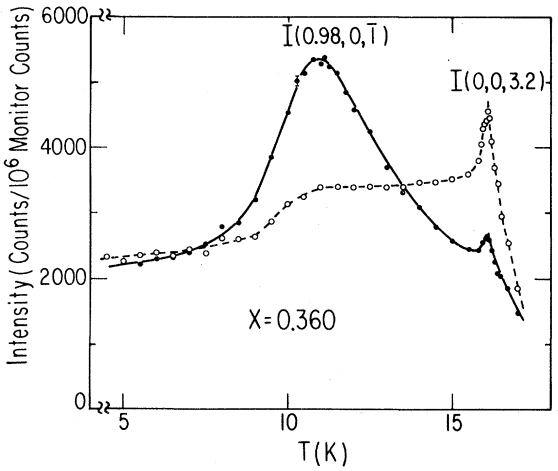

FIG. 13. Wing intensity vs temperature for concentration $x=0.360$.

respectively, $I(1,0,\bar{1})$ increases sharply where $I(0,0,9)$ was negligibly small. According to Eqs. (12a) and (12b), this indicates the ordering of $\vec{S}_{||}$ at a temperature we have defined as T_H. The small amount of rounding at T_H is primarily due to critical scattering and shows little smearing of the transition due to composition gradient. The increase of $I(0,0,9)$ below T_H is very slow; it has an inflection point at T_L, which is also visible in $I(1,0,\bar{1})$ and *suggests* some ordering of $\vec{S}_{\perp}$. But the smoothness of this data, at T_L, like the $\chi(0)$ data (Fig. 4) is not typical of a second-order phase transition. For $x \gtrsim 0.3$ the features associated with $\vec{S}_{||}$ and $\vec{S}_{\perp}$ are reversed. In Figs. 8 and 9, where $x=0.350$ and 0.360, respectively, both $I(1,0,\bar{1})$ and $I(0,0,9)$ increase rapidly below T_H thus indicating the ordering of $\vec{S}_{\perp}$. The smooth inflection point at T_L is seen only in $I(1,0,\bar{1})$, but not in $I(0,0,9)$. This therefore suggests some ordering of $\vec{S}_{||}$. In Fig. 10, where $x=0.400$, there is no sign of a lower transition and the ratio $I(1,0,\bar{1})/I(0,0,9)$ is approximately constant down to 5 K due to the ordering of $\vec{S}_{\perp}$ alone.

At the wing position of a magnetic reflection where Bragg scattering is negligible, the intensity normally originates in the diffuse scattering and gives the wave-vector–dependent susceptibilities $\chi_{||}(\vec{q})$ and $\chi_{\perp}(\vec{q})$ according to Eq. (13). In Figs. 11–13 we show the temperature dependence of the wing intensity for those samples on which the data

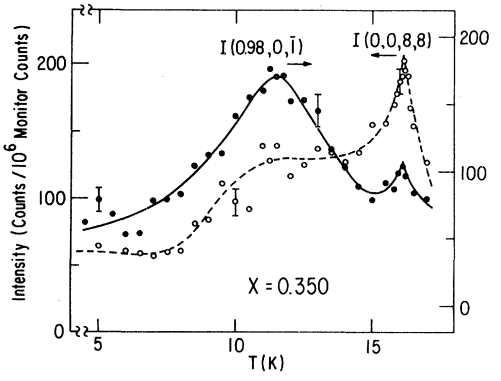

FIG. 12. Wing intensity vs temperature for concentration $x=0.350$.

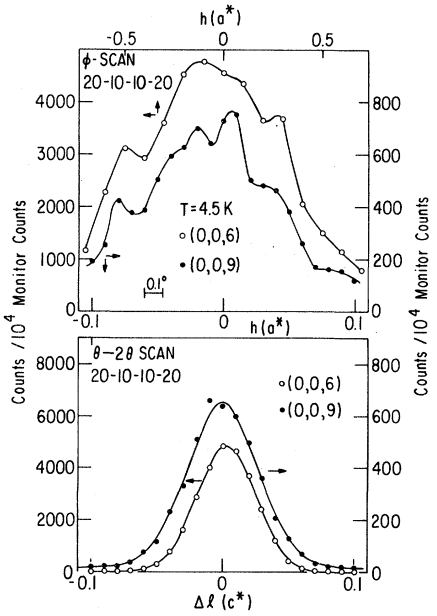

FIG. 14. Comparison of the nuclear and magnetic line shapes for concentration $x=0.275$.

in Figs. 7–9 were taken. At $x=0.291$ (Fig. 11), $\chi_{\|}(\vec{q})$ is sharply peaked at T_H, while $\chi_{\perp}(\vec{q})$ shows a broad maximum at T_L. At $x=0.350$ and 0.360 (Figs. 12 and 13), $\chi_{\perp}(\vec{q})$ is sharply peaked at T_H, while $\chi_{\|}(\vec{q})$ has a broad maximum at T_L. These features match well with those in Figs. 7–9; but more surprisingly, $\chi_{\perp}(\vec{q})$ in Figs. 12 and 13 show a gradual steplike decrease below T_L, which seems to suggest a reduction of fluctuation in $\vec{S}_{\perp}$ when $\vec{S}_{\|}$ becomes more ordered. Careful viewing of Fig. 9 reveals a very weak inflection in the corresponding peak intensity data; in Fig. 8, this is masked by the larger statistical error.

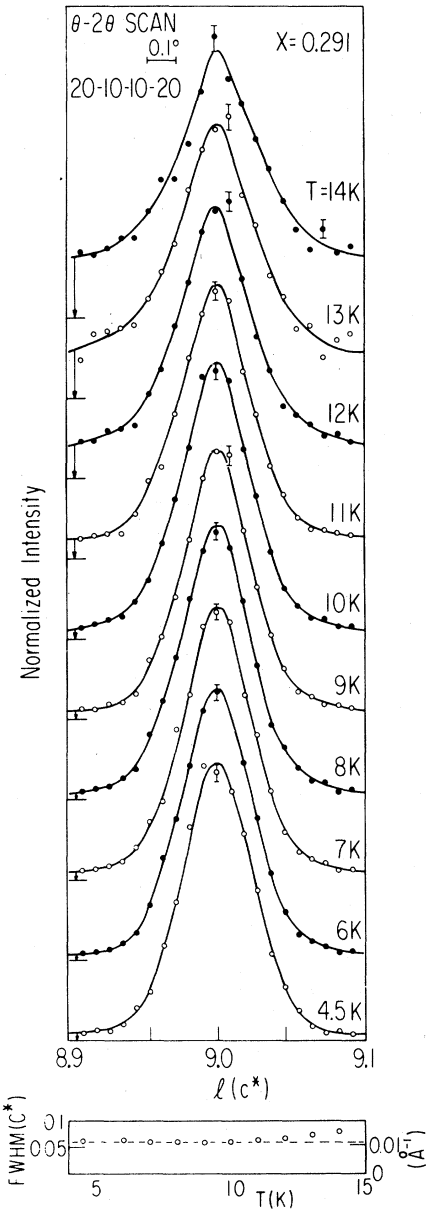

FIG. 15. Logitudinal line shapes at different temperatures for concentration $x=0.291$.

The values of T_H and T_L determined from the maximum in either I_D or $|dI_B/dT|$ (the former is usually more accurate) are listed in Table III and plotted as the open circles in Figure 3. The agreement with the susceptibility data is obviously excellent. The MCP was found to be at $x_m=0.307$ and $T_M=14.92$ K. For $x<x_M$, as the temperature is lowered, the system first enters the "$\vec{S}_{\|}$-ordered" phase at T_H and then the "mixed" phase at T_L. For $x>x_M$, the system will first enter the $\vec{S}_{\perp}$-order phase.

The smooth temperature dependence observed at T_L in both the magnetic susceptibility and neutron scattering data suggest behavior which is quite unlike that observed at normal second-order phase transitions. In this context it is important to determine whether or not T_L corresponds to a temperature associated with the development of long-range magnetic order. If the range of magnetic coherence is less than the neutron spectrometer resolution a broadened intensity profile will be observed. Because of the poor mosaicity of our sample, it is best to compare the profile of a magnetic reflection with that of a nearby nuclear reflection. In Figs. 14 and 15 we show the results of a detailed study on the $x=0.291$ sample, on which the data in Figs. 7 and 11 was taken; the lower transition is associated with $\vec{S}_{\perp}$ and (0,0,9) is the magnetic reflection of interest. In Fig. 14 we compare its intensity profile at 4.5 K to that of the (0,0,6) nuclear reflection. The ϕ scan and θ-2θ scan are in the directions a^* and c^*, respectively; they are related to the average range of coherence in the a-b plane and along the c-axis, respectively. Evidently, these profiles are resolution limited and the coherence in this case is at least a few hundred angstroms. In Fig. 15 we show the

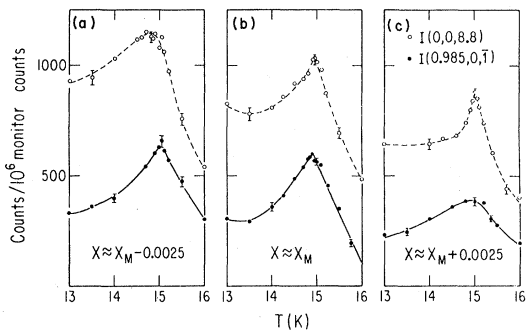

FIG. 16. Wing intensity as a function of temperature in samples with (a) $x\approx x_M-0.0025$, (b) $x\approx x_M$, and (c) $x\approx x_M+0.0025$.

normalized θ-2θ profile of the same sample at ten different temperatures below T_H, which demonstrates how the magnetic correlations evolve with temperature. We note that even at 14 K (which is well above T_L), the width is only approximately 30% above instrument resolution, and at all temperatures below T_L, it is resolution limited. These results imply that significant correlations exist in $\vec{S}_\perp$ immediately below T_H when $S_{||}$ is ordered. Similar conclusions can be inferred from the temperature dependence of the magnetic susceptibility. Thus we see no well-defined temperature where long-range order sets in but rather large magnetic correlations (or domains) which gradually increase past our instrumental resolution. Unfortunately, a similar study in samples with $x > x_M$ is not possible, since $I(1,0,\bar{1})$ is always resolution limited below T_H due to $\vec{S}_\perp$ ordering.

It is quite clear that the results described in this section are in strong disagreement with the simple theoretical arguments given in Sec. II. Most important, the lower transition lines are either nonexistent or at least drastically altered by the existence of long-range order in the other spin component. This is most clearly illustrated in Fig. 16 where we display the wing intensity in the immediate vicinity of $x_M(=0.307)$ where the upper transition lines meet. Note that at x_M (middle panel) the critical scattering associated with both $\vec{S}_{||}$ and $\vec{S}_\perp$ is relatively sharp. However, at $x_M - 0.0025$ (left panel) the phase transition associated with $\vec{S}_\perp$ is broadened while at $x_M + 0.0025$ (right panel) the transition associated with $\vec{S}_{||}$ is broadened.[3] Thus the lower transition is broadened independent of whichever component orders at T_H, or concomitantly, independent of whether the broken symmetry is discrete ($\vec{S}_{||}$) or continuous ($\vec{S}_\perp$).

It is quite clear therefore that $\vec{S}_{||}$ and $\vec{S}_\perp$ are *not decoupled* and do not behave independently. The magnetic susceptibility data in Figs. 4(c)–4(f) show $\chi_\perp$ to have a bump at T_H where $\vec{S}_{||}$ orders and $\chi_{||}$ to have a bump when $\vec{S}_\perp$ orders; neutron scattering data in Figs. 6, 7, and 11 show substantial intensity at both (0,0,9) and at (0,0,9.2) between T_H and T_L, and Fig. 16 shows convincingly that the prior existence of long-range order in either $\vec{S}_{||}$ or $\vec{S}_\perp$ has a dramatic effect on the lower transition. Figure 3 further shows that even given the uncertainties in defining T_L, the line *DM* is not a smooth extension of line *BM*, in disagreement with both the theoretical predictions of FA (Ref. 4) and the experimental conclusions of Tawaraya and co-workers.[28,29] In the section that follows we discuss the nature of the $\vec{S}_{||}$-$\vec{S}_\perp$ coupling and show how off-diagonal terms in the Hamiltonian lead to the failure of the theoretical predictions of Sec. III.

V. NONDIAGONAL EXCHANGE AND RANDOM FIELDS

In the theory of Fishman and Aharony[4] a diagonal pseudospin Hamiltonian

$$\mathcal{H}^{\mathrm{FA}} = -\sum_{\langle ij \rangle} J_{ij}^{\perp}[S_x(i)S_x(j)+S_y(i)S_y(j)] + J_{ij}^{||}S_z(i)S_z(j) \tag{14}$$

was used as the starting point. This assumes implicitly a cylindrical symmetry about the z axis and a reflection symmetry across the x-y plane. Recently, Mukamel[30] has pointed out that since the crystal structure of $FeCl_2$ and $CoCl_2$ is rhombohedral rather than hexagonal, additional higher-order terms are allowed by symmetry. Specifically, for the space group D_{3d}^5, a quartic term of the form $\vec{S}_{||}\vec{S}_\perp^3$ may occur.[30] The effects of such a term are clear. For $x > x_M = 0.307$ and $T < T_H$ this term will generate an effective longitudinal magnetic field proportional to $\langle S_\perp^3 \rangle$ acting on the $||$ component of the spin. This in turn will cause the $||$ transition to be rounded so that there will be no true phase boundary corresponding to the ordering of $S_{||}$. For $x < x_M$ and $T < T_H$, this term will generate a cubic term $S_\perp^3$ with a magnitude proportional to $\langle S_{||} \rangle$. This then places the $\perp$ transitions in the universality class of the three-component Potts model which is expected to have a weak first-order transition.

In order to assess the importance of the $S_{||}S_\perp^3$ contribution it is, of course, necessary to estimate its relative magnitude. Mukamel has suggested a mechanism for generating such a term which is a pure fluctuation effect and which decreases to zero like T^3 at low temperatures. On the other hand, we find that the rounding of the $||$ transition for $x > x_M$ *increases* with decreasing temperature so that the Mukamel mechanism cannot be dominating our experimental results. The $S_{||}S_\perp^3$ term may also arise directly from crystal-field effects. We emphasize, however, that this term is rigorously absent in the $S(\mathrm{Fe}) = 1, S(\mathrm{Co}) = \frac{1}{2}$ spin-Hamiltonian approximation and therefore can only contribute via off-diagonal coupling to the higher-lying crystal-field levels. Indeed such effects have been observed directly in pure $FeCl_2$.[31(a)] We conclude, therefore, that from crystal-field effects alone such a term will occur and it will alter the $||$ and $\perp$ phase transitions as discussed above. It is clear, on the other hand, that this will not explain the experimental results. First, it seems unlikely to us that the term, since it only occurs in higher-order perturbation theory, can ever be large enough to explain the severe rounding we observe in the low-temperature $||$ transitions for

$x > x_M$. Second, for $x < x_M$ this term generates a weak first-order character in an otherwise sharp second-order transition in $\vec{S}_\perp$. From the long correlation lengths experimentally observed for $T_L < T < T_H$ with $x < x_M$ we would expect the first-order jump to be quite small. Instead, we find that the $\vec{S}_\perp$ transition for $x < x_M$ is extremely rounded. Further, the general behavior of the $\vec{S}_\perp$ transition for $x < x_M$ is similar to that found for the $\vec{S}_{||}$ transition for $x > x_M$. It is clear therefore that it is necessary to identify an alternate mechanism to account for the observed behavior.

Our mechanism rests on the observation that although globally the symmetry is D_{3d}^5, locally there is no symmetry at all. Thus locally a number of *bilinear* off-diagonal coupling terms will occur. These terms may be as large as the exchange coupling terms in Eq. (1). We now proceed to discuss the effects of local off-diagonal coupling on the Fishman-Aharony phase diagram.

It has long been known that exchange interactions between ions with orbital degeneracy are not necessarily well represented by the usual Heisenberg form $-J\vec{S}_1\cdot\vec{S}_2$.[31(b)] The charge distribution of these ions is spatially anisotropic; their overlap (exchange) depends not just on wheter the spins are parallel or antiparallel but also on the relative orientation of the charge cloud to the displacement vector $\vec{R}_{12}$. The pseudospin vectors $\vec{S}_1$ and $\vec{S}_2$ are coupled to the charge cloud of the two ions; the electronic exchange interaction is represented by an interaction between $\vec{S}_1$ and $\vec{S}_2$. For the same $\vec{S}_1\cdot\vec{S}_2$, the amount of charge overlap is different for different $\vec{r}_{12}$ ($\vec{r}_{12}\equiv\vec{R}_{12}/|\vec{R}_{12}|$). Quite generally, one must include at least two additional terms in the Hamiltonian. In the molecular-field approximation there should be three independent components of the molecular field acting on $\vec{S}_1$ in the directions of $\vec{S}_2$, $\vec{r}_{12}$, and $(\vec{S}_2\times\vec{r}_{12})$, respectively. In a three-dimensional space, this exhausts the possibility of bilinear scalar coupling between $\vec{S}_1$ and $\vec{S}_2$. If the charge clouds are isotropic, the extra terms are unnecessary. For ions with large spin anisotropy, the charge cloud is by necessity anisotropic; hence instead of Eq. (14) the Hamiltonian should have the form

$$\mathcal{H}=-\sum_{\langle ij\rangle}J_{ij}\vec{S}(i)\cdot\vec{S}(j)+K_{ij}[\vec{r}_{ij}\cdot\vec{S}(i)][\vec{r}_{ij}\cdot\vec{S}(j)] +G_{ij}[\vec{S}(j)\times\vec{r}_{ij}]\cdot\vec{S}(i)\ , \tag{15}$$

where K_{ij} and G_{ij} are coupling constants. Equation (15) can be separated into diagonal and nondiagonal parts

$$\mathcal{H}^d=\sum_{\langle ij\rangle}[J_{ij}+(\vec{r}_{ij}^{\,x})^2K_{ij}]S_x(i)S_x(j)+[J_{ij}+(\vec{r}_{ij}^{\,y})^2K_{ij}]S_y(i)S_y(j)+[J_{ij}+(\vec{r}_{ij}^{\,z})^2K_{ij}]S_z(i)S_z(j)\ , \tag{16a}$$

$$\mathcal{H}^{\rm nd}=-\sum_{\langle ij\rangle}2K_{ij}[r_{ij}^xr_{ij}^yS_x(i)S_y(j)+r_{ij}^yr_{ij}^zS_y(i)S_z(j)+r_{ij}^zr_{ij}^xS_z(i)S_x(j)]+G_{ij}[\vec{S}(j)\times\vec{r}_{ij}]\cdot\vec{S}(i)\ . \tag{16b}$$

In classical magnetism where the mean-field approximation is always assumed, $\mathcal{H}^{\rm nd}$ is usually zero in pure systems by symmetry requirements. For example, in $FeCl_2$ or $CoCl_2$, the z axis is a threefold axis giving

$$\sum_j r_{ij}^xr_{ij}^y=\sum_j r_{ij}^yr_{ij}^z=\sum_j r_{ij}^zr_{ij}^x=0\ .$$

With $\langle\vec{S}(j)\rangle$ identical for all j, the molecular field on $\vec{S}(i)$ due to the K_{ij} term in Eq. (16b) is zero. The G_{ij} term can also be neglected because $\sum_j\vec{r}_{ij}=0$ in any crystal. Therefore, no molecular field can result from $\mathcal{H}^{\rm nd}$ in a pure system and only $\mathcal{H}^d$ needs to be considered. By noting that $(r_{ij}^x)^2=(r_{ij})^2\neq(r_{ij}^z)^2$ in the present case we see that $\mathcal{H}^d$ will take the form of $\mathcal{H}^{\rm FA}$ if we replace $(r_{ij}^x)^2$ and $(r_{ij}^y)^2$ by their average. In random systems like $Fe_{1-x}Co_xCl_2$ the above arguments are invalid since the spins are not all equivalent; $\mathcal{H}^{\rm FA}$ is then insufficient to describe the interaction and all the terms in Eqs. (15) and (16) must be considered. In the absence of any theory to deal with these terms exactly we shall make the simple molecular-field approximation to appreciate their significance. As described below, this leads to drastic changes of all the phase-transition properties, especially those associated with the lower transition.

At the lower transition, since one spin component is already ordered, we can make the mean-field approximation on that component alone and see how it affects the other component. For example, if $\vec{S}_{||}$ [$\equiv(0,0,S_z)$] is ordered, we replace $S_z(i)$ by $\langle S_z\rangle$ in Eqs. (16a) and (16b), and obtain the Hamiltonian for $\vec{S}_\perp$ [$\equiv(S_x,S_y,0)$]

$$\mathcal{H}_\perp=-\sum_{\langle ij\rangle}J_{ij}\vec{S}_\perp(i)\cdot\vec{S}_\perp(j)+K_{ij}[\vec{r}_{ij}^{\,\perp}\cdot\vec{S}_\perp(i)][\vec{r}_{ij}^{\,\perp}\cdot\vec{S}_\perp(j)]+G_{ij}[\vec{S}_\perp(i)\times\vec{S}_\perp(j)]\cdot\vec{r}_{ij}^{\,z}-\sum_i\vec{h}_\perp(i)\cdot\vec{S}_\perp(i) \tag{17a}$$

where

$$\vec{h}_{\perp}(i)=2\sum_j K_{ij}[\vec{r}^{\,z}_{ij}\cdot\langle\vec{S}_{||}(j)\rangle]\vec{r}^{\,\perp}_{ij} + G_{ij}\langle\vec{S}_{||}(j)\rangle\times\vec{r}^{\,\perp}_{ij} \ . \tag{17b}$$

Similarly, if $\vec{S}_{\perp}$ is ordered first, we replace $\vec{S}_{\perp}(i)$ by $\langle\vec{S}_{\perp}(i)\rangle$ and the Hamiltonian for $\vec{S}_{||}$ becomes

$$\mathscr{H}^{||}=-\sum_{\langle ij\rangle}[J_{ij}+K_{ij}(r^z_{ij})^2]\vec{S}_{||}(i)\cdot\vec{S}_{||}(j) - \sum_i \vec{h}_{||}(i)\cdot\vec{S}_{||}(i) \ , \tag{18a}$$

where

$$\vec{h}_{||}(i)=2\sum_j K_{ij}[\vec{r}^{\,\perp}_{ij}\cdot\langle\vec{S}_{\perp}(j)\rangle]\vec{r}^{\,z}_{ij} + G_{ij}\langle\vec{S}_{\perp}(j)\rangle\times\vec{r}^{\,\perp}_{ij} \ . \tag{18b}$$

Clearly, with random K_{ij} and G_{ij}, $\vec{h}_{\perp}(i)$ and $\vec{h}_{||}(i)$ are random in both directions and magnitude at every site. They are coupled to $\vec{S}_{\perp}(i)$ and $\vec{S}_{||}(i)$, as a static site-random applied field.

Random-field Hamiltonians have been studied extensively in recent years.[32–42] It is now generally believed that in continuous symmetry systems in the limit that the random field is less than the exchange, the field lowers the effective spatial dimensionality by 2. In other words, the upper marginal dimensionality d_u (above which mean-field theory is valid) changes from $d_u=4$ in zero field to $d_u=6$ in a random field. Similarly the lower marginal dimensionality d_c (below which no order exists) shifts from $d_c=2$ to $d_c=4$. For discrete symmetry systems the $d\rightarrow d-2$ rule is more controversial.[37–42] It is generally believed on theoretical grounds that the application of a random field to Ising model also shifts d_u from 4 to 6. Experiments on $Co_{1-x}Zn_xF_2$ and $RbCo_{1-x}Mg_xF_4$ suggest that d_c shifts from 1 to 3.[41] However, more experiments need to be done to prove the case.

For pedagogical purposes it is useful to think of the random field in terms of the domain arguments by Imry and Ma.[32] For $d\leq 4$ it is energetically favorable for a continuous symmetry system to take advantage of spatial fluctuations in the random field by breaking up into domains; the energy gain within the domain compensates for the exchange cost of generating a domain wall. For Ising spins the arguments are more complex[38] but for small enough d the results are the same: domain formation with no long-range order. It is perhaps also useful to recall that a random field is the field conjugate to the Edwards-Anderson spin-glass order parameter. Hence at any finite temperature some fraction of the spin entropy is lost with the spins partially freezing into static domains. In $Fe_{1-x}Co_xCl_2$ when $\vec{S}_{||}$ orders, it generates a random field on $\vec{S}_{\perp}$ which changes the lower marginal dimensionality for $\vec{S}_{\perp}$ to $d=4$. We expect, therefore, no long-range order in $\vec{S}_{\perp}$ at any temperature; the range of order (or domain size) is determined by the strength of the random field compared to the exchange. Similar arguments should hold for the case where $\vec{S}_{\perp}$ order prevents $\vec{S}_{||}$ order, should d_c prove to be 3 for Ising spins.

Insofar as the neutron scattering cross-section is concerned, since there is no long-range order associated with the lower transition, there should be no Bragg component. Instead there should be a *pseudo-Bragg* component related to the $[\langle S_i\rangle\cdot\langle S_j\rangle]_c$ correlation which is due to the domians. The form of the scattering cross-section associated with the pseudo-Bragg component is expected to be a squared Lorentzian with momentum space width given by the inverse domain size.[40,41] On the other hand, there is also Lorentzian diffuse scattering associated with spin fluctuations $[\langle\delta\vec{S}_i\cdot\delta\vec{S}_j\rangle]_c$, where $\delta\vec{S}_i=\vec{S}_i-\langle\vec{S}_i\rangle$. With this background all the important features in our data can be qualitatively understood as follows:

(i) Immediately below T_H, where one spin component orders, it generates a random field on the nonordering spin component and induces the formation of domains (in that component). This then should lead to an anomaly in the dc susceptibility. In fact, as shown in Fig. 4, a kink is observed in the dc susceptibility of the nonordering spin component.

(ii) The pseudo-Bragg scattering from the domains (I'_B) produces intensity profiles that are relatively narrow since the domains are of finite size. As temperature decreases, the domains should grow bigger and the profiles become narrower and eventually become resolution limited, as we observed in Fig. 15. Unfortunately, the resolution of the neutron spectrometer together with the irregular mosaicity of the samples vitiated the observation of finite spin-spin correlations at low temperatures, as well as the unusual structure factors anticipated for random-field systems.

(iii) Since the domains are large, the peak intensity at a Bragg position is due primarily to domain scattering (I'_B). The smooth temperature dependence we observed in Figs. 6–9 is thus a manifestation of the fact that a random field exists at all temperatures below T_H.

(iv) The wing intensity at the lower transition contains contributions from both I'_B and I_D. However, at the upper transition it contains only I_D. This may account for the large difference in intensity in Figs. 12 and 13.

It is important to remark that the explanations

given above are valid for both $x > x_M$ and $x < x_M$ data; regardless of whether $\vec{S}_{||}$ or $\vec{S}_{\perp}$ orders at T_H, it will produce a random field on the other spin component. This is in accord with essentially all of our experimental observations.

VI. MULTICRITICAL AND CRITICAL BEHAVIOR

It is clear from the discussion in the preceding section that the existence of a random field is able to account qualitatively for much of the observed behavior along the lower transition line T_L. Because of the off-diagonal local coupling we might also expect important effects for the upper critical lines near x_M.[2,43] Indeed, Mukamel has argued that off-diagonal coupling can make the point x_M, T_M a Heisenberg bicritical rather than a tetracritical point.[30] The crossover exponent for a Heisenberg bicritical point is $\phi = 1.25$.[44] Reasonable estimates for the range of validity of coupled Heisenberg behavior can be obtained by relating the anisotropy parameter ($g \equiv \bar{D}/\bar{J}$) to the concentration Δx ($\equiv |x - x_m|$). One finds coupled behavior for $t \lesssim 10^{-1}$ when $\Delta x < 0.06$. Therefore, it is possible to observe effective isotropic behavior in the normal critical region ($t \lesssim 10^{-1}$) if the sample concentration is within a few atomic percent of x_M. With this motivation we reexamine the behavior in the vicinity of the multicritical point x_M.

The MCP in Fig. 3 was studied in some detail using the "moving mask" method described in Sec. III. In one of the samples we surveyed (not listed in Table II), x varied approximately from 0.256 to 0.316, containing the multicritical value of $x_M = 0.307$. The sample was 1.25 in. long and x was determined for five equally spaced segments along its length; the result is shown in Fig. 17(a). The upper transition temperature for different segments of the sample was determined by measuring either the peak or wing intensity as a function of temperature. The cadmium mask was moved vertically by 0.1 in. or less for each measurement, while the opening of the horizontal slit on the mask was only about 0.07 in. The result of T_H as a function of mask position is shown in Fig. 17(b). By properly matching the positional scale between Figs. 17(a) and 17(b), T_H as a function of x was determined. This was achieved by matching the $T_H = 16.15$ K data point in Fig. 17(b) to the $x = 0.284$ data point in Fig. 17(a); it is in fact by this method that we determined $x_M = 0.307$. Combining Figs. 17(a) and 17(b), we obtained the result shown in Fig. 18(a), where T_H is plotted against x near the MCP. By taking the data points for $x < x_M$, except the one closest to x_M, we plotted Δx vs ΔT on a log-log scale

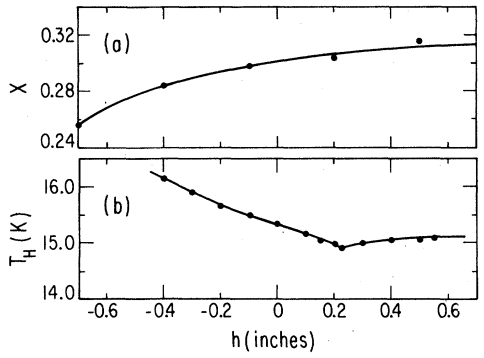

FIG. 17. Concentration and transition temperature vs position of mask along the sample.

($\Delta x \equiv |x - x_M|$, $\Delta T \equiv |T_H - T_M|$) in Fig. 18(b) and obtained a straight line with slope equal to 1.22. In other words, close to the MCP the upper phase boundary for $x \lesssim x_M$ fits well to the equation

$$\Delta x \propto \Delta T^{\phi},$$

where $\phi \simeq 1.22$ (a similar test for $x \gtrsim x_M$ has not been made). Slightly different matching of Figs. 17(a) and 17(b) would undoubtedly modify this result, but in several different attempts, we found that the log-log plot of Δx vs ΔT was always quite linear and gave ϕ in the range of 1.2–1.4, which implies that the upper phase boundaries are asymptotically tangential at the MCP. This result seems to support the conjecture that the MCP behaves *effectively* like an isotropic bicritical point with $\vec{S}_{||}$ and $\vec{S}_{\perp}$ coupled in the experimentally accessible temperature range. However, this agreement must be viewed with some

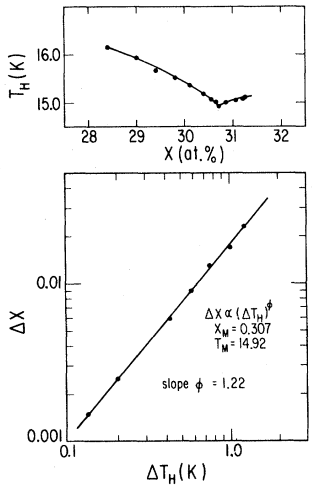

FIG. 18. Transition temperature vs concentration for x near x_M.

reservation since there are many uncertainties in the procedure we used in finding $T_H(x)$. Furthermore, we note that any amount of concavity in the phase boundaries in Fig. 18(a) would lead to a value of ϕ greater than unity. Therefore, this result should not be regarded as proof of bicritical behavior, rather, it is only suggestive.

As discussed by a number of authors,[2,43] the existence of nondiagonal terms in the Hamiltonian could conceivably affect the nature of the upper transition not only at x_M but also along the entire upper transition line. Indeed, Mukamel and Grinstein have suggested that the transition along line *MB* (in Fig. 3) should be either first order or smeared.[2] Since these transitions are all essentially continuous in our experiments, it is of interest to determine the associated critical exponents. The exponent β, which is related to the order parameter by

$$M(T) \propto t^{\beta} ,$$

where $t \equiv |(T-T_c)/T_c|$, can be readily determined from our intensity data. This is accomplished by least-square fitting $I_B(T)$ below the upper transition to the form

$$\frac{I_B(T)}{I_B(0)} = Dt^{2\beta} .$$

If $x < x_M$, $I_B(T)$ at $(1,0,\bar{1})$ gives $\beta_{||}$, which is associated with $M_{||}$; if $x > x_M$, $I_B(T)$ at either (0,0,3) or (0,0,9) gives $\beta_{\perp}$, which is associated with $M_{\perp}$. However, one must first obtain $I_B(T)$ by subtracting the critical diffuse scattering I_D from the measured intensity I. This is achieved by the following method: For every temperature T^- below T_H, we find a temperature T^+ above T_H such that the wing intensity at T^- and T^+ is approximately equal; by assuming the wing intensity is purely diffuse and $I_D(T^-)=I_D(T^+)$ at the peak position, we have

$$I_B(T^-) = I(T^-) - I_D(T^-)$$
$$= I(T^-) - I_D(T^+) .$$

By restricting ourselves to the use of only the data in the approximate reduced temperature range $10^{-1} \gtrsim t \gtrsim 10^{-2}$ for the least-squares fit, we found the critical scattering correction is generally less than 2%; it becomes much more important when $t \lesssim 10^{-2}$. In using $I_B(1,0,\bar{1})$ to find $\beta_{||}$, the Bragg scattering due to $\vec{S}_{\perp}$ must be subtracted, which can only be estimated from $I(0,0,9)$ at each temperature of interest. This prevented us from determining $\beta_{||}$ in samples with x very close to x_M; in the ones for which analyses were made, the correction was less than 1% of $I(1,0,\bar{1})$. In the actual analysis both the raw data I and the corrected data I_B were fitted to Eq. (16); several different ranges of t were tried for each fit. By observing how χ^2 changes with the fitting range, an optimum range can be decided; within this range, χ^2 is generally less than 2 but greater than 1. The resulting values of β, T_c, and D are given in Table III; they represent the average of the many different fits to the data. The error limits represent the difference among the many fits and not the result of any particular fit, which is usually much smaller. Figures 19 and 20 show two examples of these fits; they are obtained with the data shown in Figs. 3 and 7 ($x=0.275$ and 0.400, respectively) with proper subtractions. Although $\beta_{||}$ and $\beta_{\perp}$ were determined to unrealistically small uncertainty in these examples; they are undoubtedly sensitive to the sample's composition gradient, the subtraction procedure, and the choice of temperature range. The results given in Table III show that in different samples we have obtained the $\beta_{||}$ range from 0.25 to 030, and $\beta_{\perp}$ from 0.30 to 0.35; they thus agree approximately with the theoretical values $\beta_{||}=0.32$ and $\beta_{\perp}=0.35$ for $d=3$ Ising and XY transitions, respectively.[45] The results associated with the $\vec{S}_{||}$ transition ($x < x_M$) are also consistent with those obtained for pure $FeCl_2$ ($\beta=0.29\pm0.01$ and $D=1.47\pm0.02$) by Yelon and Birgeneau.[15] Therefore, within our many experimental limitations, we do not detect any significantly different new exponent close to the MCP. If the MCP is bicritical, it should have $d=3$ Heisenberg-model critical exponents. Unfortunately, the theoretical value of $\beta=0.37$ for the $d=3$ Heisenberg model[45] is too close to the 0.35 for the XY model, impossible to distinguish experimentally, and $\beta_{||}$ very near the MCP could not be determined for reasons mentioned above. Hence we can only conclude that the upper transitions are consistent with the behavior of a pure $d=3$ Ising (if $x < x_M$) or XY (if $x > x_M$) system. No evidence for either a first-order or a smeared transition has been found.

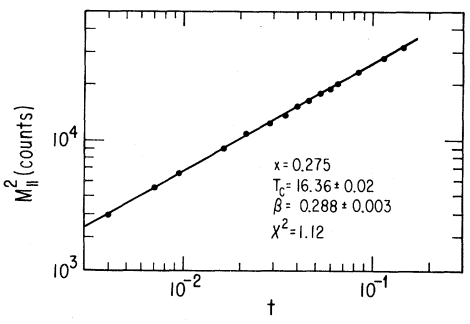

FIG. 19. Sublattice magnetization vs reduced temperature ($t=T_c-T/T_c$) for concentration $x=0.275$.

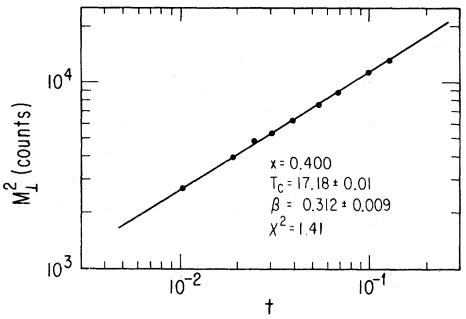

FIG. 20. Sublattice magnetization vs reduced temperature ($t = T_c - T/T_c$) for concentration $x = 0.400$.

VII. CONCLUSIONS

Over the last fifteen years mixtures of antiferromagnets with competing anisotropies have been extensively studied. Examples include $K_2Mn_{1-x}Fe_xF_4$,[46–48] $K_2Ni_{1-x}Fe_xF_4$,[49] $Rb_2Co_{1-x}Fe_xF_4$,[50] $Fe_{1-x}Co_xCl_2 \cdot 2H_2O$,[51–54] $Ni_xCo_{1-x}Cl_2 \cdot 6H_2O$,[55] $DyP_{1-x}V_xO_4$,[56] and $CsMn_{1-x}Co_xCl_3 \cdot 2H_2O$.[57] These experimental studies have been supplemented by numerous theoretical papers with the greatest emphasis being placed on mean-field calculations of the type given in Sec. III B.[58–61] It is not possible to review anthologically the literature here. In brief, essentially all the phase diagrams predicted using mean-field theory are tetracritical as shown in Fig. 3. Furthermore, the agreement between theory and the general features of the measured phase diagrams appears to be quite good. In hindsight this agreement is rather surprising given the importance of the off-diagonal coupling between the competing spin components. As we have shown above, the lower transitions of the tetracritical phase diagram do not even exist due to random molecular fields. This feature should be true for all the experimental systems listed above. We believe that the general agreement between experiment and theory reflects the fact that often the random field is small[62] and there is therefore some remnant of the lower phase boundaries.

One of the most direct demonstrations of the existence of the random-field-induced domain phase is the Mossbauer study of $Fe_{1-x}Co_xCl_2 \cdot 2H_2O$ by Ito *et al.*[54] They found that just below the upper transition both the ordering and the nonordering spin components are frozen on the Mössbauer time scale. In contrast, neutron-diffraction studies of the same system found long-range order in only one spin component.[52] Presumably the nonordering spins are frozen by the molecular field of the ordering spins. Another manifestation of the low-temperature domains is illustrated in Fig. 21. Here we show the

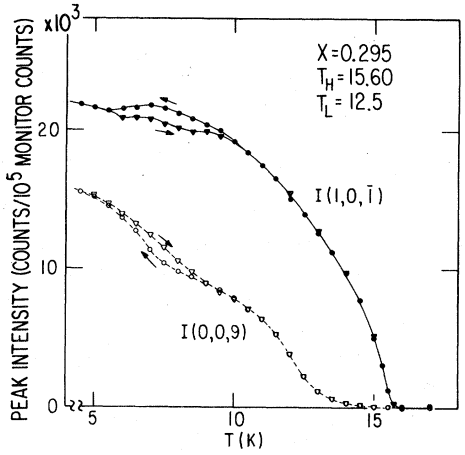

FIG. 21. Peak intensity vs temperature for concentration $x = 0.295$.

existence of low-temperature thermal hysteresis for a sample with x near x_M. Similar behavior is observed for samples with concentrations in the range $0.29 \lesssim x \lesssim 0.35$. This hysteresis is accompanied by extremely slow relaxation phenomena with time scales often over 20 min. This behavior is typical of magnets which have both a magnetoelastic coupling and a competition between various domian phases.[63]

Finally we return to the phase diagram of random anisotropy magnets. As discussed above, the lower phase boundaries in the tetracritical phase diagram are destroyed by the random fields generated by the ordered spins. What then is the nature of the phase diagram at low temperatures? By symmetry there must be some type of phase boundary separating the regions of Ising order from the regions of XY order. We believe that the most likely natue of this boundary is a line of first-order transitions resulting in a bicritical phase diagram as shown in Fig. 2(d). Unfortunately, the long correlation lengths associated with the nonordering spins, as well as the large hysteresis region mentioned above, make identification of a unique first-order line essentially impossible.

ACKNOWLEDGMENTS

The authors thank G. Grinstein, A. Aharony, D. Mukamel, and E. Pytte for many helpful discussions. We acknowledge support by the NSF under Grant No. DMR-7923203 and work at Yale under Grant No. DMR-7918175. Work at Brookhaven was supported by the Division of Basic Energy Sciences, Department of Energy under Contract No. DE-AC0Z-76CH00016. We also have benefitted from support of the Materials Research Laboratory at the University of Chicago.

*Present address: Schlumberger-Doll Research, Ridgefield, CT 06877.

[1]For a review see, e.g., A. Aharony, J. Magn. Magn. Mater. 7, 198 (1978); S. Kirkpatrick, Phys. Rev. B 16, 4630 (1977).

[2]D. Mukamel and G. Grinstein, Phys. Rev. B 25, 381 (1982).

[3]Po-zen Wong, P. M. Horn, R. J. Birgeneau, C. R. Safinya, and G. Shirane, Phys. Rev. Lett. 45, 1974 (1980).

[4]S. Fishman and A. Aharony, Phys. Rev. B 18, 3507 (1978); A. Aharony and S. Fishman, Phys. Rev. Lett. 37, 1587 (1976).

[5]For a brief review see, e.g., L. J. de Jongh and A. R. Miedema, Adv. Phys. 23, 1 (1974).

[6]R. Wyckoff, *Crystal Structures,* 2nd ed. (Interscience, New York, 1965), Vol. 1, p. 270.

[7]Po-zen Wong, J. Cryst. Growth 58, 609 (1982).

[8]M. K. Wilkinson, J. W. Cable, E. D. Wollan, and W. C. Koehler, Phys. Rev. 113, 497 (1959).

[9]I. S. Jacobs, S. Roberts, and S. D. Silverstein, J. Appl. Phys. 39, 816 (1968).

[10]R. J. Birgeneau, W. B. Yelon, E. Cohen, and J. Mackowsky, Phys. Rev. B 5, 2607 (1972).

[11]J. Kanamori, Prog. Theor. Phys. 20, 890 (1958).

[12]M. E. Lines, Phys. Rev. 131, 540 (1963).

[13]E. C. Hsu, Ph.D. dissertion, University of Chicago, 1970 (unpublished).

[14]M. T. Hutchings, J. Phys. C 6, 3143 (1973).

[15]W. B. Yelon and R. J. Birgeneau, Phys. Rev. B 5, 2615 (1972).

[16]K. Liu and M. E. Fisher, J. Low Temp. Phys. 10, 655 (1973).

[17]F. Matsubara and Inawashiro, J. Phys. Soc. Jpn. 42, 1529 (1977).

[18]A. Bruce and A. Aharony, Phys. Rev. B 11, 478 (1975).

[19]M. E. Fisher, in *Magnetism and Magnetic Materials—1974 (San Francisco),* Proceedings of the 20th Annual Conference on Magnetism and Magnetic Materials, edited by C. D. Graham, G. H. Lander, and J. J. Rhyne (AIP, New York, 1975), p. 273.

[20]A. R. King and H. Rohrer, in *Magnetism and Magnetic Materials—1975 (Philadelphia),* Proceedings of the 21st Annual Conference on Magnetism and Magnetic Materials, edited by J. J. Becker, G. H. Lander, and J. J. Rhyne (AIP, New York, 1976), p. 420.

[21]H. Rohrer and Ch. Gerber, Phys. Rev. Lett. 38, 909 (1977).

[22]A. B. Harris, J. Phys. C 7, 1671 (1974).

[23]C. L. Brandt, Ph.D. dissertation, University of Chicago, 1960 (unpublished).

[24]C. Trapp, Ph.D. dissertion, University of Chicago, 1963 (unpublished).

[25]R. C. Chisholm and J. W. Stout, J. Chem. Phys. 36, 972 (1962).

[26]M. E. Fisher, Philos. Mag. 7, 1731 (1962).

[27]W. Marshall and S. W. Lovesey, *Theory of Thermal Neutron Scattering* (Oxford University Press, New York, 1971).

[28]T. Tawaraya and Katsumata, Solid State Commun. 32, 337 (1979).

[29]T. Tawarya, K. Katsumata, and H. Yoshizawer, J. Phys. Soc. Jpn. 49, 1299 (1980).

[30]D. Mukamel, Phys. Rev. Lett. 46, 845 (1981).

[31](a) A. N. Bazhan and V. A. Ul'yanov, Zh. Eksp. Teor. Fiz. 79, 186 (1980) [Sov. Phys.—JETP 52, 94 (1980)]; (b) R. J. Elliott and M. F. Thorpe, J. Appl. Phys. 39, 802 (1968).

[32]Y. Imry and S. K. Ma, Phys. Rev. Lett. 35, 1399 (1975).

[33]A. Aharony, Y. Imry, and S. K. Ma, Phys. Rev. Lett. 37, 1364 (1976).

[34]G. Grinstein, Phys. Rev. Lett. 37, 944 (1976).

[35]A. P. Young, J. Phys. C 10, L257 (1977).

[36]G. Parisi and N. Sourlas, Phys. Rev. Lett. 43, 744 (1979).

[37]E. Pytte, Y. Imry, and D. Mukamel, Phys. Rev. Lett. 46, 1173 (1981).

[38]K. Binder, Y. Imry, and E. Pytte, Phys. Rev. B 24, 6736 (1981).

[39]H. S. Kogon and D. J. Wallace, J. Phys. A 14, L527 (1981).

[40]D. Mukamel and E. Pytte, Phys. Rev. B 25, 4779 (1982).

[41]H. Yoshizawa, R. A. Cowley, G. Shirane, R. J. Birgeneau, H. J. Guggenheim, and H. Ikeda, Phys. Rev. Lett. 48, 438 (1982).

[42]G. Grinstein and S. K. Ma, Phys. Rev. Lett. 49, 685 (1982).

[43]A. Aharony, Solid State Commun. 28, 661 (1978).

[44]J. M. Kosterlitz, D. R. Nelson, and M. E. Fisher, Phys. Rev. B 13, 412 (1976).

[45]The theoretical exponents in three dimensions are tabulated by D. J. Wallace, in *Phase Transitions and Critical Phenomena,* edited by C. Domb and M. S. Green (Academic, London, 1976), pp. 294–357.

[46]L. Bevaart, J. V. Lebesque, E. Frikkee, and L. J. de Jongh, Physica (Utrecht) 86-88B, 729 (1977); L. Bevaart, E. Frikkee, J. V. Lebesque, and L. J. de Jongh, Solid State Commun. 25, 1031 (1978).

[47]L. Bevaart, E. Frikkee, and L. J. de Jongh, Solid State Commun. 25, 1031 (1978).

[48]L. Bevaart, E. Frikkee, J. V. Lebesque, and L. J. de Jongh, Phys. Rev. B 18, 3376 (1978).

[49]A. Ito *et al.*, presented at the Annual Meeting of the Physical Society of Japan, Fukui, 1980 (unpublished).

[50]Y. Someya *et al.*, presented at the Annual Meeting of the Physical Society of Japan, Tokyo, 1980 (unpublished).

[51]K. Katsumata, M. Kobayaski, T. Sato, and Y. Miyaka, Phys. Rev. B 19, 2700 (1979).

[52]K. Katsumata, M. Kobayaski, and H. Yoshizawa, Phys. Rev. Lett. 43, 960 (1979).

[53]M. Kobayaski, K. Katsumata, T. Sato, and Y. Miyako, J. Phys. Soc. Jpn. 46, 1467 (1979).

[54]A. Ito, Y. Someya, and K. Katsumata, Solid State Commun. 36, 681 (1980).

[55]K. Takeda, M. Matsuura, and T. Haseda, J. Phys. Soc.

Jpn. 29, 885 (1970).
[56]P. Kettler, M. Steiner, H. Dachs, R. Germer, and B. Wankyln, Phys. Rev. Lett. 47, 1329 (1981).
[57]I. Yamamoto, K. Nagata, T. Sato, and Y. Miyako, J. Magn. Magn. Mater. 15-18, 251 (1960).
[58]F. Matsubara and S. Inawashiro, J. Phys. Soc. Jpn. 42, 1529 (1977).
[59]F. Matsubara and S. Inawashiro, J. Phys. Soc. Jpn. 46, 1740 (1979).
[60]Y. Someya, J. Phys. Soc. Jpn. 50, 3897 (1981).
[61]Y. Someya and T. Tamaki, Natl. Sci. Rep. Ochanomizu Univ. 32, 87 (1981).
[62]K. Nakanishi (unpublished).
[63]See, for example, R. J. Birgeneau, H. J. Guggenheim, and G. Shirane, Phys. Rev. B 1, 2211 (1970).